Exciton states in spherical parabolic GaAs quantum dots

1996 J. Phys.: Condens. Matter 8 5725

(http://iopscience.iop.org/0953-8984/8/31/006)

J. Phys.: Condens. Matter **8** (1996) 5725–5735. Printed in the UK

Exciton states in spherical parabolic GaAs quantum dots

T Garm

Institute of Physics, University of Aalborg, Pontoppidanstræde 103, DK-9220 Aalborg Øst, Denmark

Received 22 February 1996, in final form 22 April 1996

Abstract. The lowest (s, S) and (p, P) exciton states of a GaAs quantum dot with an isotropic parabolic potential are calculated. Hole states are calculated from the Luttinger–Kohn scheme in the spherical approximation, thus taking light-hole and heavy-hole mixing into account. Exciton states are obtained from an expansion of the wavefunction in a basis formed by products of electron and hole states, and the size dependence of the exciton levels is investigated. By comparison to a one-band model it is found that the effect of valence band mixing is very important and that the one-band model overestimates the exciton energy by more than 20% in the case of strong confinement.

1. Introduction

The progress in nanoscale lithography and microcrystallite doping of glasses now makes it possible to study the dynamics of confined carriers in zero-dimensional systems. Optical spectroscopic measurements have proven very successful in investigations of the effects of size quantization on electron and hole states in these systems. Far-infrared transmission spectroscopy on quantum dot (QD) samples of GaAs, InSb and related structures (see, e.g., [1–3]) have clearly demonstrated size quantization in intersubband transitions. These studies, as well as theoretical ones [4], indicate that the in-plane confinement is approximately parabolic (harmonic). The properties of interband transitions have mainly been investigated for the cases of CdS and CdSe microcrystallites embedded in a dielectric [5–9]. Due to the sharp boundary between materials these systems are well described by a spherical square-well potential [6, 9]. A few reports have published luminescence spectra for interband transitions in QDs of GaAs and related compounds. The earliest of these [10, 11] were hampered by large inhomogeneous broadening due to the size distribution of the nanostructures, and even though size quantization was clearly demonstrated details of the level structure could not be obtained. Recently, however, Brunner *et al* [12] have published data from interband photoluminescence experiments performed on single GaAs/AlGaAs QDs prepared by thermal interdiffusion. These results show well-resolved exciton peaks in the luminescence spectra and the size dependence of the exciton levels are extracted. Again, it is found that the confinement is approximately parabolic.

A number of theoretical investigations of exciton levels in GaAs QDs have been published. The importance of the Coulomb attraction has been demonstrated [13, 14]. These studies, however, used a simple one-band model for the valence band. The effects of valence band mixing in GaAs QDs have been studied in [15] and [16]. Here, square-well potentials (spherical and box-type) are assumed and the conclusion is that valence

0953-8984/96/315725+11$19.50

band mixing is very important for both geometries. The effects of valence band mixing in more realistic potentials, however, have not been studied. In the case of QDs prepared by thermal interdiffusion starting from a narrow quantum well, the potential is presumably well described by a hard-wall potential in the direction perpendicular to the quantum well and a soft confinement potential in the plane. Unfortunately, even for cylindrical geometry a full valence-band-mixing calculation is very complicated. Hence, in the present work we will take a spherical parabolic potential to represent the confinement. This type of potential is assumed to be adequate in the case of interdiffusion starting from a quantum well of width comparable to the range of the interdiffusion profile, i.e. much larger then the 30 Å width of the sample used by Brunner *et al.* In addition, restricting ourselves to such wide potentials ensures the applicability of the effective-mass approximation (EMA) since the EMA is only valid for potentials with a large extent compared to the lattice constant. In the case of a GaAs microcrystallite in vacuum, Ramaniah and Nair [17] showed that the EMA is quite inadequate in the size range of 8–28 Å radius considered by them. In the present model the confinement is produced by the interdiffusion profile, i.e. a smoothly varying Al concentration in an infinite medium. Hence, the restriction on the EMA may be somewhat relaxed but obviously the EMA cannot be used uncritically. Also, as demonstrated in [9], the assumption of a slowly varying envelope potential superimposed on the lattice potential is inadequate for the smallest QDs. Hence, even though the present theory will be formulated with the particle diameter (d) as a variable parameter, the region where $d <$ effective Bohr radius is actually outside the presumed limits of validity.

In the case of spherical symmetry the Luttinger–Kohn [18] Hamiltonian may be simplified dramatically [19, 20]. Baldereschi and Lipari [20] showed that on retaining only the spherically symmetric part of the Hamiltonian, the hole state Schrödinger equation reduces to two coupled radial equations. Thus, this scheme is easily handled by numerical methods. In this paper we adopt the spherical approximation for the calculation of hole states, and electron states are calculated from a simple single-band model. Using the joint basis of electron and hole states, exciton states are found by introducing the Coulomb coupling between electrons and holes. Numerical results for GaAs are presented and the full valence-band-mixing calculation is compared to the one-band model used by Que [14]. The two results for the exciton ground-state energy are shown to differ significantly in the cases of intermediate and strong confinement.

2. Electron and hole states

Our model assumes a slowly varying Al fraction in the otherwise homogeneous GaAlAs medium to be responsible for the QD potential. Hence, complications arising from boundaries between media with different dielectric constants can be neglected, and we will take a purely parabolic potential to represent the confinement. A natural complication arises from the fact that the parabolic potential $V(r) = \frac{1}{2}m\omega_0^2 r^2$ has an explicit dependence on the effective mass in question. Hence, electrons in different valence bands will experience different confinement potentials. In addition, the confinement introduces mixing between the valence bands, so mixed states rather than decoupled light- and heavy-hole states are observed. This leads to some arbitrariness in the choice of mass for the potential. This difficulty could be removed via introduction of different parabola frequencies for electrons and holes (say, ω_0 and Ω_0) and use of these as independent fitting parameters. Here, however, we will follow the lines of Que [14] and use the same parabola frequency for both holes and electrons. Also, it is assumed that the lowest size-quantized levels are adequately described using the light-hole mass in the potential. Consequently, the potentials felt by

electrons and holes are taken to be spherically symmetric and given by $V_e(r) = \frac{1}{2}m_e\omega_0^2 r^2$ and $V_h(r) = \frac{1}{2}m_{lh}\omega_0^2 r^2$, respectively, where m_e and m_{lh} are the effective electron and light-hole masses and ω_0 is the common parabola frequency. The assumption of identical parabola frequencies implies that for materials with $m_{lh} \approx m_e$, such as GaAs, the range of electron and hole potentials will be approximately equal. Hence, a large overlap between electron and hole wavefunctions is expected and Coulomb coupling will be strong. If, on the other hand, widely different parabola frequencies were used, the coupling would be reduced which in turn would lead to reduced binding energies and oscillator strengths. Using identical parabola frequencies but widely different masses would lead to a similar result.

All states are (sums of) products of a Bloch part and an envelope part. Throughout we take $\boldsymbol{r}$ to mean the position vector in envelope space, and so $\langle \boldsymbol{r}|\psi\rangle$ denotes the projection of $|\psi\rangle$ onto envelope space. The envelope wavefunctions of electron states are $\varphi_{n,l,m}(\boldsymbol{r}) = Y_{lm}(\theta,\varphi)R_{n,l}(r)$, with $R_{n,l}(r)$ satisfying the radial equation

$$\left[-\frac{\hbar^2}{2m_e}\frac{1}{r}\frac{\mathrm{d}^2}{\mathrm{d}r^2}r + \frac{1}{2}m_e\omega_0^2 r^2 + \frac{l(l+1)\hbar}{2m_e r^2}\right]R_{n,l}(r) = E_{n,l}R_{n,l}(r). \tag{1}$$

We will restrict this treatment to the lowest s- and p-type states and for notational simplicity we relabel the s- and p-type radial functions according to $R_{n,0}(r) \equiv l_n(r)$ and $R_{n,1}(r) \equiv k_n(r)$. The normalized radial part of the wavefunctions is given by

$$l_n(r) = \beta^{3/2}\left(\frac{2n!}{\Gamma(n+3/2)}\right)^{1/2} L_n^{1/2}(\beta^2 r^2)\mathrm{e}^{-(1/2)\beta^2 r^2} \tag{2}$$

and

$$\begin{aligned} k_n(r) &= \beta^{3/2}\left(\frac{2n!}{\Gamma(n+5/2)}\right)^{1/2} \beta r L_n^{3/2}(\beta^2 r^2)\mathrm{e}^{-(1/2)\beta^2 r^2} \\ &= \frac{1}{\beta r}\left\{(n+3/2)^{1/2}l_n(r) - (n+1)^{1/2}l_{n+1}(r)\right\} \end{aligned} \tag{3}$$

where $\beta = (m_e\omega_0/\hbar)^{1/2}$, and the corresponding energy eigenvalues are $E_{n,0} = (\frac{3}{2}+2n)\hbar\omega_0$ and $E_{n,1} = (\frac{5}{2}+2n)\hbar\omega_0$, respectively. The hole states are labelled by the total angular momentum $\boldsymbol{F}$, the principle quantum number N and the envelope angular momenta. In fact, each state contains two terms with envelope angular momentum L and $L+2$, respectively, and so mixing between these different angular momenta is observed [9, 15]. The lowest states are the S-like ($L = 0$) and P-like ($L = 1$) states with $F = 3/2$. These states are labelled $\left|N\mathrm{S}_{F_z}\right\rangle$ and $\left|N\mathrm{P}_{F_z}\right\rangle$ and can be expressed as [15, 20]

$$\left\langle r|N\mathrm{S}_{F_z}\right\rangle = f_{N\mathrm{S}}(r)\,|0, 3/2, 3/2, F_z\rangle + g_{N\mathrm{S}}(r)\,|2, 3/2, 3/2, F_z\rangle \tag{4}$$

and

$$\left\langle r|N\mathrm{P}_{F_z}\right\rangle = f_{N\mathrm{P}}(r)\,|1, 3/2, 3/2, F_z\rangle + g_{N\mathrm{P}}(r)\,|3, 3/2, 3/2, F_z\rangle\,. \tag{5}$$

Here the angular dependence is incorporated via the $|L, J, F, F_z\rangle$ states, where J is the Bloch function angular momentum and F_z is the component of $\boldsymbol{F}$ in the z-direction. In the general Luttinger–Kohn scheme the valence band is described by three effective-mass parameters γ_1, γ_2 and γ_3, but in the spherical approximation the isotropy assumption $\gamma_2 = \gamma_3$ is used. These parameters enter via the effective hole mass $m_h = m_0/\gamma_1$, and the spin–orbit coupling $\mu = 2\gamma_2/\gamma_1$. In fact, the assumption $\gamma_2 = \gamma_3$ is only strictly needed for the spherically non-invariant part of the Luttinger–Kohn Hamiltonian. Retaining $\gamma_2 \neq \gamma_3$ in the spherically invariant part (axial approximation) simply implies using [20] $\mu = (6\gamma_3 + 4\gamma_2)/5\gamma_1$ as

the strength of the spin–orbit coupling. Hence, the difference between the two degrees of approximation only lies in the choice of μ to be used in numerical calculations. In terms of the spin–orbit coupling the light-hole mass is given by $m_{lh} = m_h/(1+\mu)$. When using simplified length and energy units taken as β^{-1} and $\frac{1}{2}\hbar\omega_0$, respectively, the radial functions are solutions to the following set of coupled differential equations [15, 20]:

$$\begin{bmatrix} -\frac{1}{\gamma}\left[\frac{\mathrm{d}^2}{\mathrm{d}r^2}+\frac{2}{r}\frac{\mathrm{d}}{\mathrm{d}r}\right]+\frac{\gamma}{1+\mu}r^2-E_{N\mathrm{S}} & \frac{\mu}{\gamma}\left[\frac{\mathrm{d}^2}{\mathrm{d}r^2}+\frac{5}{r}\frac{\mathrm{d}}{\mathrm{d}r}+\frac{3}{r^2}\right] \\ \frac{\mu}{\gamma}\left[\frac{\mathrm{d}^2}{\mathrm{d}r^2}-\frac{1}{r}\frac{\mathrm{d}}{\mathrm{d}r}\right] & -\frac{1}{\gamma}\left[\frac{\mathrm{d}^2}{\mathrm{d}r^2}+\frac{2}{r}\frac{\mathrm{d}}{\mathrm{d}r}-\frac{6}{r^2}\right]+\frac{\gamma}{1+\mu}r^2-E_{N\mathrm{S}} \end{bmatrix} \times \begin{bmatrix} f_{N\mathrm{S}}(r) \\ g_{N\mathrm{S}}(r) \end{bmatrix} = 0 \tag{6}$$

and

$$\begin{bmatrix} -\left(\frac{1}{\gamma}-\frac{4\mu}{5\gamma}\right)\left[\frac{\mathrm{d}^2}{\mathrm{d}r^2}+\frac{2}{r}\frac{\mathrm{d}}{\mathrm{d}r}-\frac{2}{r^2}\right]+X & \frac{3\mu}{5\gamma}\left[\frac{\mathrm{d}^2}{\mathrm{d}r^2}+\frac{7}{r}\frac{\mathrm{d}}{\mathrm{d}r}+\frac{8}{r^2}\right] \\ \frac{3\mu}{5\gamma}\left[\frac{\mathrm{d}^2}{\mathrm{d}r^2}-\frac{3}{r}\frac{\mathrm{d}}{\mathrm{d}r}+\frac{3}{r^2}\right] & -\left(\frac{1}{\gamma}+\frac{4\mu}{5\gamma}\right)\left[\frac{\mathrm{d}^2}{\mathrm{d}r^2}+\frac{2}{r}\frac{\mathrm{d}}{\mathrm{d}r}-\frac{12}{r^2}\right]+X \end{bmatrix} \times \begin{bmatrix} f_{N\mathrm{P}}(r) \\ g_{N\mathrm{P}}(r) \end{bmatrix} = 0 \tag{7}$$

where

$$X = \frac{\gamma}{1+\mu}r^2 - E_{N\mathrm{P}}$$

where $\gamma = m_h/m_e$. The additional factor $1/(1+\mu)$ in the parabolic terms corresponds to the use of the light-hole mass for the confinement potential, as argued above. The size dependence of the energy eigenvalues $E_{N\mathrm{S}}$ and $E_{N\mathrm{P}}$ is hidden in the choice of energy units as is seen from the relation $\frac{1}{2}\hbar\omega_0 = \hbar^2\beta^2/2m_e$, i.e. the energy eigenvalues scale as (length scale)$^{-2}$. It may be noted that without the presence of the confinement, the solutions to the equations above are given in terms of spherical Bessel functions with eigenvalues proportional to $1+\mu$ and $1-\mu$ corresponding to decoupled light- and heavy-hole states, respectively. The radial functions of the $|N\mathrm{S}_{F_z}\rangle$ and $|N\mathrm{P}_{F_z}\rangle$ states are obtained from an expansion in a finite basis. For later convenience, the orthonormal bases $\{l_i(r)\}$ and $\{k_i(r)\}$ are chosen. Hence, solving equations (6) and (7) reduces to calculating the coefficients $\{a_i, b_i, c_i, d_i\}$ given by

$$f_{N\mathrm{S}}(r) = \sum_i a_i l_i(r) \qquad \text{and} \qquad g_{N\mathrm{S}}(r) = \sum_i b_i l_i(r) \tag{8}$$

and

$$f_{N\mathrm{P}}(r) = \sum_i c_i k_i(r) \qquad \text{and} \qquad g_{N\mathrm{P}}(r) = \sum_i d_i k_i(r) \tag{9}$$

subject to the normalization conditions

$$\sum_i (a_i^2 + b_i^2) = 1 \qquad \text{and} \qquad \sum_i (c_i^2 + d_i^2) = 1.$$

The expressions (8) and (9) are inserted into the coupled differential equations, each of which are then transformed into a single matrix equation from which the eigenvalues and eigenvectors are obtained numerically.

3. Exciton states

We now introduce the Coulomb coupling between electrons and holes. The Coulomb interaction conserves the total angular momentum but not that of the individual particles. Consequently, this leads to coupling between sS and pP electron–hole pairs. Since the total angular momentum is a good quantum number, the exciton wavefunction is conveniently expanded in a basis consisting of eigenstates of the total angular momentum. In optical spectroscopy, spin-conserving transitions are dominating and so the exciton state should have vanishing total spin. Hence, we will restrict this treatment to exciton states with a total angular momentum $\boldsymbol{\mathcal{F}}$ characterized by $\mathcal{F} = 1$ and $\mathcal{F}_z = 0$. We take $\mathcal{N} = 0, 1, \ldots$ to label the exciton level, and the exciton states $|\Phi_{\mathcal{N}}\rangle$ are expanded as follows:

$$|\Phi_{\mathcal{N}}\rangle = \sum_{n,N} C_{nN}\,|n\mathrm{s}N\mathrm{S}\rangle + \sum_{n,N} D_{nN}\,|n\mathrm{p}N\mathrm{P}\rangle\,. \tag{10}$$

If we denote the electron Bloch wavefunction by $|\mathrm{S}\sigma\rangle$, $\sigma \in \{-1/2, 1/2\} = \{\downarrow, \uparrow\}$, the basis states are given by

$$\begin{aligned}|n\mathrm{s}N\mathrm{S}\rangle &= \sum_{F_z,\sigma} \left|\varphi_{n,0,0}\right\rangle |\mathrm{S}\sigma\rangle \left|N\mathrm{S}_{F_z}\right\rangle (1/2\ \sigma\ 3/2\ F_z|1\ \ 0) \\ &= \frac{1}{\sqrt{2}} \left|\varphi_{n,0,0}\right\rangle \left\{|\mathrm{S}\uparrow\rangle \left|N\mathrm{S}_{-1/2}\right\rangle - |\mathrm{S}\downarrow\rangle \left|N\mathrm{S}_{1/2}\right\rangle\right\}\end{aligned} \tag{11}$$

and

$$\begin{aligned}|n\mathrm{p}N\mathrm{P}\rangle = &\sum_{F_z,\sigma,m} \left|\varphi_{n,1,m}\right\rangle |\mathrm{S}\sigma\rangle \left|N\mathrm{P}_{F_z}\right\rangle (1\ m\ 1/2\ \sigma|3/2\ \ -F_z)(3/2\ \ \sigma+m\ \ 3/2\ F_z|1\ \ 0) \\ &= \frac{1}{\sqrt{60}} \left\{3\sqrt{3}\left|\varphi_{n,1,-1}\right\rangle \left|N\mathrm{P}_{3/2}\right\rangle - \sqrt{2}\left|\varphi_{n,1,0}\right\rangle \left|N\mathrm{P}_{1/2}\right\rangle - \left|\varphi_{n,1,1}\right\rangle \left|N\mathrm{P}_{-1/2}\right\rangle\right\} |\mathrm{S}\downarrow\rangle \\ &\quad + \frac{1}{\sqrt{60}} \left\{3\sqrt{3}\left|\varphi_{n,1,1}\right\rangle \left|N\mathrm{P}_{-3/2}\right\rangle\right. \\ &\quad \left. - \sqrt{2}\left|\varphi_{n,1,0}\right\rangle \left|N\mathrm{P}_{-1/2}\right\rangle - \left|\varphi_{n,1,-1}\right\rangle \left|N\mathrm{P}_{1/2}\right\rangle\right\} |\mathrm{S}\uparrow\rangle\end{aligned} \tag{12}$$

where $(j_1\ \ m_1\ \ j_2\ \ m_2|j\ \ m)$ is the Clebsch–Gordan coefficient for addition of angular momenta. Provided that we use energy units of $\frac{1}{2}\hbar\omega_0$, the exciton problem reduces to calculating eigenvalues and eigenvectors of the Hamiltonian matrix with elements

$$H_{nN,mM} = (E_n + E_N)\delta_{nm}\delta_{NM} - \lambda R_{nN,mM} \tag{13}$$

where $\lambda = 2/(a_0^*\beta)$ is the ratio between the QD diameter $d \approx 2/\beta$ and the effective electron Bohr radius $a_0^* = 4\pi\epsilon\epsilon_0\hbar^2/(e^2 m_e)$, ϵ being the static dielectric constant of GaAs. In addition, the $R_{nN,mM}$-matrix contains the Coulomb matrix elements. This matrix is conveniently written in terms of four submatrices corresponding to whether the electron–hole pairs are of s or p type, i.e.

$$R_{nN,mM} = \begin{pmatrix} R^{\mathrm{ss}}_{nN,mM} & R^{\mathrm{sp}}_{nN,mM} \\ R^{\mathrm{ps}}_{nN,mM} & R^{\mathrm{pp}}_{nN,mM} \end{pmatrix} \tag{14}$$

where, for instance,

$$R^{\mathrm{ss}}_{nN,mM} = \langle n\mathrm{s}N\mathrm{S}|\,\frac{1}{\beta r_{eh}}\,|m\mathrm{s}M\mathrm{S}\rangle\,. \tag{15}$$

The matrix elements are calculated using the central result [21]

$$\frac{1}{|\boldsymbol{x}-\boldsymbol{y}|}=4\pi\sum_{k=0}^{\infty}\sum_{m=-k}^{k}\frac{1}{2k+1}\frac{[\min(x,y)]^k}{[\max(x,y)]^{k+1}}Y_{km}^*(\Omega_x)Y_{km}(\Omega_y) \tag{16}$$

where Ω_x is the solid angle of $\boldsymbol{x}$ etc. Using some results from the theory of angular momentum [21], the matrix elements $R_{nN,mM}$ can be expressed by the rather simple expressions

$$R^{\mathrm{ss}}_{nN,mM}=\sum_{i,j}(a_ia_j+b_ib_j)\int_0^\infty S^0_{nm}(x)l_i(x)l_j(x)x^2\,\mathrm{d}x \tag{17}$$

$$R^{\mathrm{sp}}_{nN,mM}=\sum_{i,j}\left\{\frac{2}{9}a_ic_j+\frac{8}{45}b_ic_j-\frac{8}{105}b_id_j\right\}\int_0^\infty S^1_{nm}(x)l_i(x)k_j(x)x^2\,\mathrm{d}x \tag{18}$$

$$R^{\mathrm{ps}}_{nN,mM}=\sum_{i,j}\left\{\frac{2}{9}a_jc_i+\frac{8}{45}b_jc_i-\frac{8}{105}b_jd_i\right\}\int_0^\infty S^1_{mn}(x)k_i(x)l_j(x)x^2\,\mathrm{d}x \tag{19}$$

and

$$R^{\mathrm{pp}}_{nN,mM}=\sum_{i,j}(c_ic_j+d_id_j)\int_0^\infty S^2_{nm}(x)k_i(x)k_j(x)x^2\,\mathrm{d}x \tag{20}$$

where $\{a_i,b_i,c_i,d_i\}$ and $\{a_j,b_j,c_j,d_j\}$ should be taken as the coefficients corresponding to $|nN\rangle$ and $|mM\rangle$, respectively. In the expression for $R^{\mathrm{pp}}_{nN,mM}$ a small correction stemming from the $k=2$ term in equation (16) has been neglected. In order to provide expressions for the S-functions we introduce the notation

$$S[\alpha,\beta,\gamma,\delta;x]=\sum_{a=0}^{n}\sum_{b=0}^{m}\frac{(-1)^{a+b}[n!m!\Gamma(n+\alpha)\Gamma(m+\beta)]^{1/2}}{(n-a)!(m-b)!\Gamma(a+\alpha)\Gamma(b+\beta)a!b!}$$
$$\times\left\{\frac{\Gamma(a+b+\beta)-\Gamma(a+b+\beta,x^2)}{x^{1+\delta}}+x^\delta\Gamma(a+b+\gamma,x^2)\right\} \tag{21}$$

where $\Gamma(k,z)$ is the incomplete Gamma function. Thus,

$$S^0_{nm}(x)=\int_0^\infty l_n(y)l_m(y)\frac{y^2}{\max(x,y)}\,\mathrm{d}y=S[3/2,3/2,1,0;x] \tag{22}$$

$$S^1_{nm}(x)=\int_0^\infty l_n(y)k_m(y)\frac{y^2\min(x,y)}{[\max(x,y)]^2}\,\mathrm{d}y=S[3/2,5/2,1,1;x] \tag{23}$$

and

$$S^2_{nm}(x)=\int_0^\infty k_n(y)k_m(y)\frac{y^2}{\max(x,y)}\,\mathrm{d}y=S[5/2,5/2,2,0;x]. \tag{24}$$

The above expressions can for each $\{n,m\}$ be reduced to a combination of the functions $\Phi(x)/x$, $\Phi(x)/x^2$ and $x^k\mathrm{e}^{-x^2}$. Hence, in the calculation of $R_{nN,mM}$ only three types of integral appear. These integrals are discussed in the appendix.

4. Numerical results

The computational scheme presented in the previous section is easily implemented on a computer provided that the basis set is limited to a reasonable number of states. Here we will use a 51-member basis in the calculation of hole states. Since the strength of electron and hole potentials is quite similar in the case of GaAs, hole states are easily

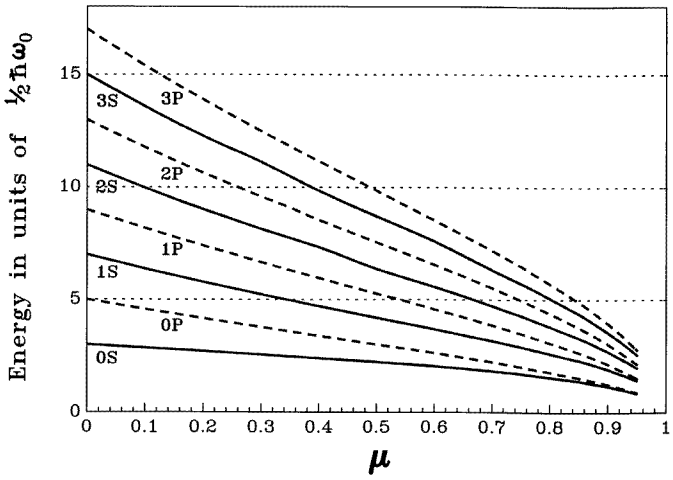

Figure 1. The four lowest $S_{F=3/2}$ (solid lines) and $P_{F=3/2}$ (dashed lines) hole state eigenvalues as a function of μ, the spin–orbit coupling. The results are obtained from a numerical solution of the coupled equations in the spherical two-band model.

constructed from a basis of electron states and convergence is fast. From usual GaAs material parameters, i.e. $m_e = 0.068m_0$ and [15] $\gamma_1 = 6.8$, we find $\gamma = 2.16$. Using these values the hole state energy eigenvalues are calculated as a function of the spin–orbit coupling μ as shown in figure 1. In the case of vanishing mixing, the decoupled light- and heavy-hole eigenvalues would scale as $1 + \mu$ and $1 - \mu$, respectively. From the actual calculation it is seen that the dependence is approximately linear in the region of small coupling, i.e. of the form $E(\mu) = E(0)(1 + \alpha\mu)$. The slope ($\alpha$), however, is somewhere between -1 and $+1$ (approximately -0.5 for the lowest state) and for large coupling the relation is no longer linear. The appropriate value of μ for GaAs is [15] $\mu \approx 0.7$ and around this value the deviation from the simple decoupled behaviour is pronounced. In addition, the energy levels are no longer equidistant. For $\mu = 0.7$ the seven lowest eigenvalues for the S states are 1.83, 3.17, 4.72, 6.32, 8.05, 9.69 and 11.4, all in units of $\frac{1}{2}\hbar\omega_0$. For the P states the corresponding values are 2.23, 3.87, 5.52, 7.18, 8.81, 10.5 and 12.2.

Once the hole states are obtained the exciton problem can be addressed. The evaluation of the $R_{nN,mM}$-matrix is somewhat time-consuming but this need only be done once due to the simple dependence on QD size of the $H_{nN,mM}$-matrix in equation (13). We take the 10 lowest electron states and 14 lowest hole states into account, so $H_{nN,mN}$ is of dimension 70×70. Using this matrix the size dependence of the energy eigenvalues is obtained numerically. In the limit $d \to 0$ ($\lambda \to 0$) the Coulomb coupling is excluded by the infinitely large confinement energy. Hence, the exciton wavefunction is simply the product of a single electron state and a single hole state, i.e. only a single term in equation (10). The exciton states are conveniently labelled by this term and so the ground state is denoted as (0s, 0S), etc. The four lowest energy eigenvalues are displayed in figure 2. Here the total exciton energy is calculated and the exciton binding energy can be obtained by subtracting the value at $d = 0$. The energy unit $\frac{1}{2}\hbar\omega_0$ can be converted into physical units using $\frac{1}{2}\hbar\omega_0 = (4/\lambda^2)R^*$, where R^* is the effective electron Rydberg $R^* \approx 4.8$ meV. In figure 3 the energy eigenvalues are shown using physical units. The effect of size quantization is seen to be very important when the QD size is comparable to the effective Bohr radius.

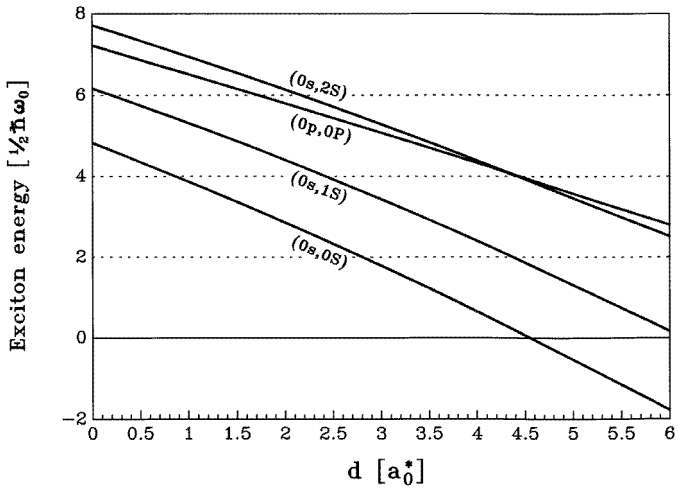

Figure 2. The four lowest exciton levels versus d, the quantum dot diameter. The energy is given in the size-dependent units $\frac{1}{2}\hbar\omega_0$.

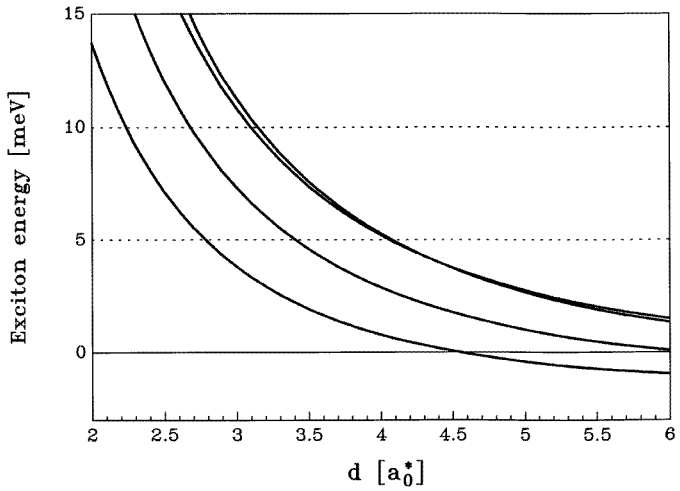

Figure 3. The same as figure 2 except that physical units of energy are used.

In order to illustrate the effect of valence band mixing on the exciton states we compare our results to those found in the model of Que [14]. In this model hole and electron states are described by single bands and, by separating centre-of-mass and relative motion, it is found that the exciton problem is reduced to solving the following equation:

$$\left[-\frac{1}{r}\frac{\mathrm{d}^2}{\mathrm{d}r^2}r + r^2 - \frac{\kappa}{r} - (E-3)\right]\phi(r) = 0. \tag{25}$$

Here $\phi(r)$ is the relative-motion part of the exciton ground-state wavefunction, r being the relative distance $r = |\boldsymbol{r}_e - \boldsymbol{r}_h|$. In addition, E is the total energy in units of $\frac{1}{2}\hbar\omega_0$ and $(m_r\omega_0/\hbar)^{1/2} \equiv 1$, m_r being the reduced mass $m_r^{-1} = m_e^{-1} + (1+\mu)m_h^{-1}$. The parameter κ

is related to the quantity λ used in the present work via $\kappa = (m_r/m_e)^{1/2}\lambda \approx 0.75\lambda$. Instead of solving the radial equation numerically, we use the variational *ansatz* $\phi(r) = A\mathrm{e}^{-r^2/2-\alpha r}$, where A is a normalization constant and α is a variational parameter determined by minimizing the energy. It is readily found that

$$E = 6 - \alpha^2 - 2\alpha\frac{\rho_3(\alpha)}{\rho_2(\alpha)} + (2\alpha - \kappa)\frac{\rho_1(\alpha)}{\rho_2(\alpha)} \tag{26}$$

where

$$\rho_n(\alpha) = \int_0^\infty \mathrm{e}^{-r^2-2\alpha r} r^n \, \mathrm{d}r. \tag{27}$$

The expression for the energy is easily minimized on a computer. Obviously, the variational energy is exact in the limits $\kappa \to 0$ and $\kappa \to \infty$. In order to check the *ansatz* for intermediate κ-values we apply the variational treatment to the spherical Zeeman problem [22]. This case is exactly identical to equation (25) provided that $\kappa = 2$ and r^2 is replaced by $2r^2$. The exact ground-state energy quoted in [22] is $E = 3.593\,77$. Using the *ansatz* $\phi(r) = A\mathrm{e}^{-r^2/\sqrt{2}-\alpha r}$ yields the result $E = 3.599\,97$. Hence, in this case the error is seen to be less than 1%. This demonstrates the validity of the variational approach used in the present work.

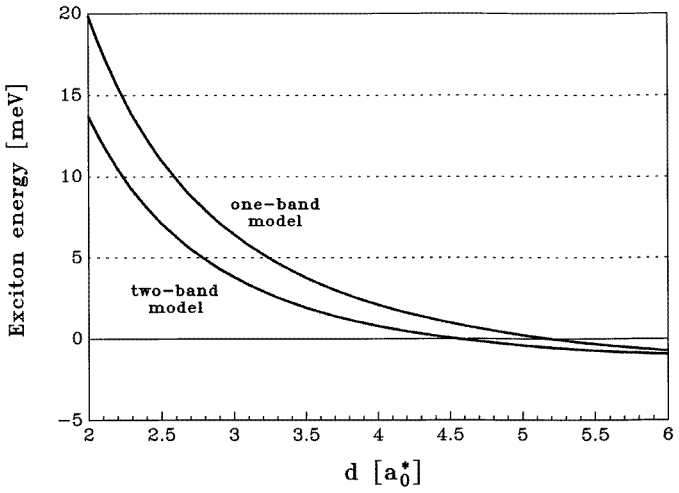

Figure 4. A comparison of the exciton ground-state energy as obtained from the full two-band model and the one-band model. The two-band result is obtained from a finite-basis expansion and the one-band result is calculated from a variational treatment.

The one-band ground-state energy obtained from the variational treatment can be compared to the two-band calculation including valence band mixing. The two results are shown together in figure 4. The different calculations are seen to converge in the limit of vanishing confinement, as expected. For strong and intermediate confinement, however, the difference is pronounced. Apparently, the one-band model in general overestimates the exciton energy. For $d = a_0^*$ and $d = 2a_0^*$ the difference between the energy eigenvalues obtained in the two models is $5.0R^*$ and $1.3R^*$, respectively, and in general for $d \leqslant 2a_0^*$ the ratio between the difference and the average energy exceeds 20%, demonstrating the significance of valence band mixing for strong confinement. It should be remembered, however, that since the present work relies on the effective-mass approximation, the results cannot be expected to hold in the case of extremely small QDs, i.e. for $d < a_0^*$.

5. Summary

In summary, we have demonstrated the importance of valence band mixing in spherical harmonic GaAs quantum dots. Starting from the spherical model of Baldereschi and Lipari [20] we have calculated hole state wavefunctions and energy eigenvalues. Using the joint basis of electron and hole states, the lowest (s, S) and (p, P) exciton levels are computed. The size dependence shows a very large enhancement of the exciton energy in the strong-confinement limit. In order to quantify the effect of valence band mixing due to the confinement, we compare our results with the one-band model of Que [14]. It is shown that the one-band model in general overestimates the exciton energy. The difference between the energy eigenvalues (normalized to the average value) found in the two approaches is large in both the strong- and intermediate-confinement regions, reaching more than 20% for the ground state in the strong-confinement limit.

Appendix. Integrals

In this appendix, explicit expressions for the integrals involved in the calculation of the $R_{nN,mM}$-matrix are presented. When the last equality of equation (3) is used it is seen that all integrals can be reduced to combinations of the expressions

$$U_{ij}^{k} = \int_0^\infty l_i(x) l_j(x) \Phi(x) x^{2k-1}\, \mathrm{d}x \qquad k = 0, 1 \tag{A1}$$

and

$$V_{ij}^{k} = \int_0^\infty l_i(x) l_j(x) \mathrm{e}^{-x^2} x^{2k+2}\, \mathrm{d}x \qquad k = -1, 0, 1, \ldots, 8. \tag{A2}$$

The computations are simplified through the recursive relations

$$U_{ij}^{0} = \left(\frac{16j^2 - 8j + 1}{2j(2j+1)}\right)^{1/2} U_{i,j-1}^{0} - \left(\frac{2}{j(2j+1)}\right)^{1/2} U_{i,j-1}^{1} - \left(\frac{(2j-1)(j-1)}{j(2j+1)}\right)^{1/2} U_{i,j-2}^{0} \tag{A3}$$

and

$$V_{ij}^{k} = \left(\frac{16j^2 - 8j + 1}{2j(2j+1)}\right)^{1/2} V_{i,j-1}^{k} - \left(\frac{2}{j(2j+1)}\right)^{1/2} V_{i,j-1}^{k+1} - \left(\frac{(2j-1)(j-1)}{j(2j+1)}\right)^{1/2} V_{i,j-2}^{k}. \tag{A4}$$

By expanding the Laguerre polynomials it is readily found that

$$U_{ij}^{1} = \sum_{a=0}^{i} \sum_{b=0}^{j} \frac{(-1)^{a+b}[i!\,j!\,\Gamma(i+3/2)\Gamma(j+3/2)]^{1/2}}{(i-a)!(j-b)!\Gamma(a+3/2)\Gamma(b+3/2)a!b!} \times \frac{2}{\sqrt{\pi}} \Gamma(a+b+3/2)\, {}_2F_1\left[\frac{1}{2}, a+b+\frac{3}{2}; \frac{3}{2}, -1\right] \tag{A5}$$

where ${}_2F_1$ is the hypergeometric function. If we introduce the notation

$$f_{ij}^{k} = \frac{(-1)^{i+j}\Gamma(i+j-k+3/2)\Gamma(i-j+k+1/2)\Gamma(j-i+k+1/2)}{\pi\, 2^{i+j-k+3/2}[i!\,j!\,\Gamma(i+3/2)\Gamma(j+3/2)]^{1/2}} \tag{A6}$$

the integral V_{ij}^8 can be expressed as

$$V_{ij}^8 = \frac{1}{2^{16}}\left[f_{ij}^8 + 240 f_{ij}^7 + 21\,840 f_{ij}^6 + 960\,960 f_{ij}^5 + 216\,216\,00 f_{ij}^4 + 242\,161\,920 f_{ij}^3 + 1210\,809\,600 f_{ij}^2 + 2075\,673\,600 f_{ij}^1 + 518\,918\,400 f_{ij}^0\right]. \tag{A7}$$

In addition to these expressions we need the results

$$U_{i0}^0 = \left(\frac{(2i+1)!}{\pi\, 2^{2i-3}}\right)^{1/2} \sum_{a=0}^{i} \frac{(-1)^a}{(i-a)!a!(a+1/2)}\, {}_2F_1\left[\frac{1}{2}, 1-a; \frac{3}{2}, \frac{1}{2}\right] \tag{A8}$$

and

$$V_{i0}^k = \frac{\Gamma(k+3/2)\Gamma(i+3/2)}{\pi[(2i+1)!\, 2^{2k-1}]^{1/2}}\, {}_2F_1\left[-i, -k; \frac{3}{2}, -1\right]. \tag{A9}$$

References

[1] Sikorski C and Merkt U 1989 *Phys. Rev. Lett.* **62** 2164
[2] Demel T, Heitmann D, Grambow P and Ploog K 1990 *Phys. Rev. Lett.* **64** 788
[3] Meurer B, Heitmann D and Ploog K 1992 *Phys. Rev. Lett.* **68** 1371
[4] Kumar A, Laux S E and Stern F 1990 *Phys. Rev.* B **42** 5166
[5] Shum K, Wang W B, Alfano R R and Jones K M 1992 *Phys. Rev. Lett.* **68** 3904
[6] Ekimov A I, Hache F, Schanne-Klein M C, Ricard D, Flytzanis C, Kudryavtsev I A, Yazeva T V, Rodina A V and Efros Al L 1993 *J. Opt. Soc. Am.* B **10** 100
[7] Bawendi M G, Wilson W L, Rothberg L, Carroll P J, Jedju T M, Steigerwald M L and Brus L E 1990 *Phys. Rev. Lett.* **65** 1623
[8] Wang Y and Herron N 1990 *Phys. Rev.* B **42** 7253
[9] Norris D J, Sacra A, Murray C B and Bawendi M G 1994 *Phys. Rev. Lett.* **72** 2612
[10] Kash K, Scherer A, Worlock J M, Craighead H G and Tamargo M C 1986 *Appl. Phys. Lett.* B **49** 1043
[11] Temkin H, Dolan G J, Panish M B and Chu S N G 1987 *Appl. Phys. Lett.* B **50** 413
[12] Brunner K, Bockelmann U, Abstreiter G, Walther M, Böhm G, Tränkle G and Weimann G 1992 *Phys. Rev. Lett.* **69** 3216
[13] Adolph B, Glutsch S and Bechstedt F 1993 *Phys. Rev.* B **48** 15 077
[14] Que W 1992 *Solid State Commun.* B **81** 721
[15] Xia J B 1989 *Phys. Rev.* B **40** 8500
[16] Willatzen M, Tanaka T, Arakawa Y and Singh J 1994 *IEEE J. Quantum Electron.* **30** 640
[17] Ramaniah L M and Nair S V 1995 *Physica* B **212** 245
[18] Luttinger J M and Kohn W 1955 *Phys. Rev.* **97** 869
[19] Sheka V I and Sheka D I 1967 *Sov. Phys.–JETP* **24** 975
[20] Baldereschi A and Lipari N O 1973 *Phys. Rev.* B **8** 2697
[21] Weissbluth M 1978 *Atoms and Molecules* (New York: Academic)
[22] Handy C R and Bessis D 1985 *Phys. Rev. Lett.* B **55** 931